PRECLINICAL AND CLINICAL SPECTROSCOPY – Full Papers

Magnetic Resonance in Medicine 78:1296–1305 (2017)

Intracerebral Synthesis of Glutamine From Hyperpolarized Glutamate

Leslie Mazuel,[1,2] Rolf F. Schulte,[3] Aurélie Cladière,[4] Claudine Spéziale,[4] Marie Lagrée,[5] Martin Leremboure,[6] Betty Jean,[4] Franck Durif,[1,7] and Carine Chassain[4]*

Purpose: Changes in glutamate (Glu) levels occur in a number of neurodegenerative diseases. We proposed the use of ^{13}C spectroscopy and the highly amplified signal generated by hyperpolarization to achieve spatial and temporal resolutions adequate for in vivo studies of Glu metabolism in the healthy rat brain. Thus, we investigated uptake of hyperpolarized [1-^{13C}]Glu after a temporary blood–brain barrier (BBB) disruption protocol and its conversion to glutamine (Gln) in the brain.

Methods: [1-^{13}C]Glu was hyperpolarized using the dynamic nuclear polarization process. A temporary BBB disruption using mannitol allowed hyperpolarized [1-^{13}C]Glu to reach the brain. Then, hyperpolarized [1-^{13}C]Glu brain metabolism was observed in vivo by MR spectroscopy experiments at 3T. Products synthesized from [1-^{13}C]Glu were assigned via liquid chromatography–mass spectrometry.

Results: Hyperpolarized [1-^{13}C]Glu reached 20% ± 2.3% polarization after 90 min. After validation of the BBB disruption protocol, hyperpolarized [1-^{13}C]Glu (175.4 ppm) was detected inside the rat brain, and the formation of [1-^{13}C]Gln at 174.9 ppm was also observed.

Conclusion: The Gln synthesis from hyperpolarized [1-^{13}C]Glu can be monitored in vivo in the healthy rat brain after opening the BBB. **Magn Reson Med 78:1296–1305, 2017. © 2016 International Society for Magnetic Resonance in Medicine.**

Key words: dynamic nuclear polarization; ^{13}C MR spectroscopy; hyperpolarized [1-^{13}C]glutamate; blood–brain barrier disruption; glutamate metabolism

INTRODUCTION

Current understanding of the roles that glutamate (Glu) and glutamine (Gln) play in the central nervous system seems to indicate that a disturbance in the Glu–Gln equilibrium may be involved in mental illness, tumor development, and neurodegeneration (1). However, the exact relationship between this imbalance and subsequent pathologies is not fully understood. This has generated an increased interest in Glu and Gln quantifications in the healthy brain as well as in brain diseases. Short echo time proton magnetic resonance spectroscopy (^{1}H MRS) is a powerful in vivo technique for detecting and quantifying brain metabolites such as Glu and Gln. For example, ^{1}H MRS studies have shown that changes in Glu levels may be involved in neurodegenerative diseases such as Parkinson disease (2,3) and Alzheimer's disease (4). Given the toxicity of excess Glu and the essential role of the astrocytic Gln synthase in Glu clearance, it is therefore of interest to assess the Glu–Gln metabolism in vivo. However, real-time in vivo study of the Glu–Gln metabolism remains a challenge.

Carbon-13 MRS (^{13}C MRS) is an informative tool to study the brain metabolism in vivo. However, the low gyromagnetic ratio and low natural abundance of ^{13}C lead to poor sensitivity. To increase the ^{13}C MRS sensitivity in vivo, prior infusions of ^{13}C-enriched compounds combined with long acquisition times are needed, though a drawback is temporal resolution loss (5–7).

Dynamic nuclear polarization (DNP) applied to ^{13}C compounds and combined with dissolution have partially overcome the problem of ^{13}C MRS detection by boosting its sensitivity. Indeed, DNP enables up to a 10,000-fold increase in the ^{13}C signal, thus enabling real-time visualization of metabolism with high sensitivity, providing unique information about the enzymatic processes (8–10). However, the short half-life of the polarized signal restricts the signal detection in time, so care must be taken to choose the best ^{13}C-labeled precursor (11).

To date, [1-^{13}C]pyruvate is still the most widely hyperpolarized compound used because of its long T_1 relaxation time and its key role in cellular energy metabolism. However, the use of [1-^{13}C]pyruvate is restricted: the downstream metabolism of [1-^{13}C]pyruvate through the tricarboxylic acid (TCA) cycle cannot be observed, as the C_1-labeled carbon is transferred to CO_2 when the TCA cycle precursor acetyl-coenzyme A is formed. Therefore, the use of other TCA precursors, such as [2-^{13}C]pyruvate and [1-^{13}C]acetate, has been advocated to study this metabolic pathway in the

[1]Auvergne University, UFR Medicine, EA7280, Clermont-Ferrand, France.
[2]Centre de Résonance Magnétique des Systèmes Biologiques, UMR 5536, Victor Segalen University, CNRS, Bordeaux, France.
[3]GE Global Research, Munich, Germany.
[4]CHU Gabriel Montpied, MRI Department, Clermont-Ferrand, France.
[5]Plateforme d'Exploration du Métabolisme, Institut de Chimie de Clermont-Ferrand, Aubière, France.
[6]Mass Spectrometry Department, Institut de Chimie de Clermont-Ferrand, Aubière, France.
[7]CHU Gabriel Montpied, Neurology Department, Clermont-Ferrand, France.
Grant sponsor: Auvergne Region; Grant number: CPER 2007–2013.
*Correspondence to: Carine Chassain, PhD, CHU Gabriel Montpied, MRI Department, 58, rue Montalembert, 63003 Clermont-Ferrand, France.
E-mail: carine.chasssain@inra.fr
Received 26 May 2016; revised 16 September 2016; accepted 30 September 2016
DOI 10.1002/mrm.26522
Published online 8 November 2016 in Wiley Online Library (wileyonlinelibrary.com).

rodent brain. Whereas hyperpolarized experiments on the direct TCA cycle precursor [1-^{13}C]acetate allowed only the detection of 2-oxoglutarate (12), a study on [2-^{13}C]pyruvate showed the appearance of various TCA cycle intermediates up to [5-^{13}C]Glu synthesis in vivo in the rat brain (13). However, this result was not observed by other groups studying the same brain metabolism (14).

In order to observe further steps in the TCA cycle and directly related synthesis, such as the Glu and Gln syntheses, hyperpolarization of new precursors has been used. In particular, a recent report describes the indirect visualization of Glu synthesis with the use of hyperpolarized 2-ketoisocaproate (15). In a recent study, the use of hyperpolarized [1-^{13}C]α-ketoglutarate (AKG) was achieved with the synthesis of [1-^{13}C]2-hydroxyglutarate (16,17) and [1-^{13}C]Glu (17) in the rat brain. However, the Gln synthesis was below the detection levels (17). Thus, to date, the synthesis of Gln from Glu has not been detected in the brain in real time.

The aim of this study was to investigate uptake of hyperpolarized [1-^{13}C]Glu after a temporary blood–brain barrier (BBB) disruption protocol and to investigate its conversion to Gln in the rat brain.

METHODS

Hyperpolarization of [1-^{13}C]Glu

[1-^{13}C]Glu was polarized as described previously (18). Briefly, [1-^{13}C]Glu (38 mM; Sigma-Aldrich, Saint-Quentin-Fallavier, France) was dissolved in a mixture of water with 5.4 M Trizma base (Sigma-Aldrich), 20 mM of the stable trityl radical OX63 (GE Healthcare, Waukesha, Wisconsin, USA), and 1.55 mM of a gadolinium chelate (Dotarem, Guerbert, Roissy-en-France, France). The sample was sonicated and vortexed until the contents were fully dissolved. A volume of 30 μL was polarized using a HyperSense polarizer (Oxford Instruments, Oxfordshire, United Kingdom) for 90 min (3.35 T, 1.4 K, 94.101 GHz). After hyperpolarization, the frozen sample was quickly dissolved in 4 mL of a 40-mM phosphate buffer at pH 7.4. The phosphate buffer also contained 100 mg · L^{-1} disodium salts of ethylenediaminetetraacetic acid (Sigma-Aldrich), sodium (Na^+), and potassium (K^+) chloride to yield a final Na^+ concentration of 140 mM and a final K^+ concentration of 4 mM. It was heated to 180 °C and pressurized to 10 bar before dissolving the sample.

Relaxation Times and Polarization Level

Experiments were performed on a 3T MR750 Scanner (GE Healthcare). A head rodent dual-tuned (^{1}H/^{13}C) quadrature volume coil (inner diameter, 30 mm; Rapid Biomedical, Rimpar, Germany) was used for radiofrequency excitation and signal reception at 127.7 MHz and 32.1 MHz, respectively. Three ^{13}C experiments were performed to measure the mean polarization level and relaxation time. Immediately after dissolution, hyperpolarized [1-^{13}C]Glu was placed in a 1-mL syringe. ^{13}C spectra were acquired using a flip angle of 5° and a repetition time (TR) of 1000 ms. A total of 100 scans were acquired to follow the decay of the polarization. The relaxation time T_1 of hyperpolarized [1-^{13}C]Glu was determined by performing a monoexponential fit to the signal decay curve of the hyperpolarized compound. After the complete decay of the hyperpolarized signal, a spectrum was acquired at thermal equilibrum with nearly identical parameters using a 90° flip angle and a TR of 1500 ms. Adding 1.5 mmol · L^{-1} of gadolinium chelate to the hyperpolarized solution shortened the T_1 of the solution. The level of polarization in the solution was calculated by comparing the first hyperpolarized spectrum with its corresponding thermal spectrum, correcting for flip angle and number of scans. The amplitude of the hyperpolarized signal was also corrected for T_1 relaxation during the transfer time from the polarizer to the spectrometer (12 s).

Animals

All the experiments were performed on young adult male Sprague–Dawley rats weighing 180–200 g. The design, analysis, and reporting were in compliance with the Animal Research: Reporting in Vivo Experiments guidelines. The experiments complied with the European Communities Council Directive of November 24, 1986 (86/609/EEC). Protocols met the ethical guidelines of the French Ministry of Agriculture and Forests and were approved by the CEMEAA (Comite d'Ethique pour l'Experimentation Animal d'Auvergne) and registered as CE08-11. Four animals were housed per cage and maintained on a 12-h light/dark cycle at a constant temperature (21°C ± 1°C) with free access to food and water. In total, 25 different rats were used and divided into two groups (Supporting Fig. S1). Eight rats were used for ex vivo validation of the BBB disruption (n = 4 with an intracarotid injection of 0.9% NaCl and n = 4 with an intracarotid injection of a hypertonic solution of 25% mannitol 250 mg · mL^{-1}). Eleven rats were used for in vivo ^{13}C MR studies (n = 5 with an intracarotid injection of NaCl then hyperpolarized [1-^{13}C]Glu and n = 6 with an intracarotid mannitol injection then hyperpolarized [1-^{13}C]Glu). Six rats were used to validate [1-^{13}C]Glu detection in the brain using liquid chromatography–mass spectroscopy (LC-MS) analysis of brain extracts.Four rats received an intracarotid injection of mannitol followed by an injection of [1-^{13}C]Glu, and two control rats received an intracarotid injection of mannitol followed by an injection of 0.9% NaCl.

BBB Disruption

For surgical procedures, rats were anesthetized with 2%–2.5% isoflurane in air and oxygen (1.0 L · min^{-1}; 70% air and 30% oxygen). One catheter was secured in the femoral vein for injection of the intravenous anesthetic propofol (Propofol-Lipuro 1%, 10 mg · mL^{-1}; B. Braun, Boulogne-Billancourt, France). The isoflurane anesthesia was switched to propofol anesthesia, 1.2 mg · kg^{-1} · min^{-1} under 100% O_2 for the remainder of the experiment. Another catheter was secured in the right carotid artery for infusion of the hypertonic solution of 25% mannitol (infusion rate: 0.25 mL · s^{-1} · kg^{-1} for 30 s). The external carotid was ligated to maximize the delivery of mannitol toward the brain. Before delivery, the mannitol solution was heated to 37 °C and filtered using a 0.45 μm filter to prevent microinfarcts due to the possible presence of crystals.

To validate ex vivo BBB disruption, 5 min after mannitol delivery, four animals received an intracarotid injection of Evans Blue (2 mg · kg^{-1}). The other four rats received infusions of NaCl (0.5 mL · s^{-1} · kg^{-1} for 30 s) followed 5 min

later by an intracarotid injection of Evans Blue. The rats were then sacrificed. Brains were removed and extracted in formamide. Evans Blue dye in the infused hemi-brain was measured by spectrophotometry at 620 nm.

In Vivo MR Protocol

All measurements were performed using a 3T MR750 scanner. Animals under propofol anesthesia were secured in a handling system with the head centered in the coil. The respiratory rate was monitored throughout the session, and corporal temperature was maintained at 37.8 °C using a warm air system.

Anatomical imaging was performed to assess brain location using a 3D T_1-weighted sequence with the following parameters: echo time = 3.9, TR = 8800 ms, field of view = $40 \times 40\,mm^2$, matrix size = 160×160, slice thickness = 1.6 mm, acquisition time = 7 min, 40 s. For ^{13}C acquisitions, flip angle and frequency calibration were performed on a 0.5-mL tube of 3 M [1-^{13}C]lactate placed close to the head (19). A shimming procedure was performed manually, and the line width of [1-^{13}C]Glu was 15–20 Hz on average.

Two ^{13}C MRS sessions were performed. In the first session, a ^{13}C 2D dynamic chemical shift imaging (CSI) using a spectral–spatial (SPSP) excitation combined with a single-shot readout was used to visualize the [1-^{13}C]Glu in the rat brain. Five rats were separated into two groups. Three rats received mannitol and 5 min later received another injection of hyperpolarized [1-^{13}C]Glu. The other two rats received an injection of NaCl first, followed by the injection of hyperpolarized [1-^{13}C]Glu. Intracarotid injection began within 12 s after dissolution. A volume of 0.2 mL of the hyperpolarized solution was injected over 10 s. SPSP excitations started at the beginning of the hyperpolarized [1-^{13}C]Glu injection.

The specific SPSP scheme used for the RF excitation pulses (20) was designed to provide a flip angle of 15° for hyperpolarized [1-^{13}C]Glu and 90° for lactate (Lac), with a TR of 1000 ms and 64 number of scans (NS). Excitation frequencies were centered on C_1 Glu and Lac. After spectral and slice selective excitation of a single metabolite, the image was encoded with a single-shot spiral. The spiral trajectory duration was 45 ms, and a nominal matrix size of 32×32 was used. With an assumed in vivo line width on a ^{13}C frequency of 15 Hz and a matched filter of another 15 Hz, this led to a real matrix size of 16×16, which is equivalent to a pixel size of $5 \times 5\,mm^2$. ^{13}C data sets were postprocessed using a routine implemented in MATLAB (MathWorks, Natick, Massachusetts, USA) as described previously (20,21). Briefly, the integrals of [1-^{13}C]Lac and hyperpolarized [1-^{13}C]Glu were calculated. The 2D ^{13}C CSI data were superimposed on the axial T_1-weighted images to localize the brain voxels. Color heat maps of hyperpolarized [1-^{13}C]Glu were generated at the beginning of the injection by spatial interpolation of the 2D ^{13}C CSI data at the anatomical image resolution. The signal intensity was measured on the image in two regions of interest, one covering the brain and the other within the carotid artery.

In the second ^{13}C MRS session, slice-selective spectra were acquired to observe the synthesis of [1-^{13}C]Gln from hyperpolarized [1-^{13}C]Glu. Six rats were separated into two groups. Three rats received a mannitol injection and subsequently the hyperpolarized [1-^{13}C]Glu after 5 min. The other three rats received an NaCl injection followed by a hyperpolarized [1-^{13}C]Glu injection. Data acquisitions started 7 s after the beginning of the hyperpolarized [1-^{13}C]Glu injection to preserve the hyperpolarized signal and increase the chance to detect the synthetized metabolite [1-^{13}C]Gln.

Spectra were acquired using a slice-selective ^{13}C acquisition sequence covering the rat head (slice thickness = 15 mm; TR = 1000 ms; bandwidth = 4000 Hz; number of scans = 20). A small flip angle of 15° was used to preserve substrate magnetization. Integrals of hyperpolarized [1-^{13}C]Glu, [1-^{13}C]Gln, and [5-^{13}C]Glu and integral of [1-^{13}C]Lac phantom were quantified by peak integration of the dynamic hyperpolarized ^{13}C spectra using jMRUI software and the AMARES algorithm (version 5.0, http://www.mrui.uab.es/mrui). Supporting Figure S2 shows an example of fitting.

LC-MS Detection

To validate the [1-^{13}C]Glu detection inside the rat brain and the visualization of its metabolite [1-^{13}C]Gln, six rats were used and separated into two groups. Four rats received intracarotid injection of mannitol followed by an injection of [1-^{13}C]Glu, and two control rats received an intracarotid injection of mannitol followed by an injection of 0.9% NaCl under propofol anesthesia. The animals were sacrificed 5 min after [1-^{13}C]Glu or NaCl administration, and the brain was removed quickly. Brains were frozen in liquid nitrogen and stored at –80 °C until brain extraction.

Tissue extraction

Reagent-grade methanol and chloroform (4 °C) in a ratio of 2:1 (v/v; $3\,mL \cdot g^{-1}$ tissue) were added to the frozen tissue. After approximately 15 min of contact with the first solvents, chloroform and distilled water were added to the samples in a ratio of 1:1 ($1\,mL \cdot g^{-1}$ tissue) to form an emulsion. The samples were then centrifuged at 13,000 rpm for 20 min. The upper phase (methanol and water) was separated from the lower (organic) phase, and both fractions were dried at room temperature under a stream of nitrogen gas.

Analysis

All dried extract samples were redissolved and chromatographic separations were performed on a 1200 series fast-LC system (Agilent Technologies, Waldbronn, Germany) equipped with a binary solvent delivery system and an autosampler. The fast-LC system was coupled to a time-of-flight mass spectrometer (Bruker Daltonique, Wissembourg, France) equipped with an electrospray source operating in positive ion mode. Separation was performed on an UPTISPHERE CS Evolution HILIC hit column (150×2.1 mm, 2.6 µm) (Interchim, Montluçon, France). The mobile phase was composed of water (phase A) and acetonitrile (phase B) (containing 0.1% formic acid). The gradient elution was optimized as follows: 0–1 min, 100% B; 1–4 min, 100%–56% B; 4–6 min, 56%–50% B; 6–9 min, 50%–0% B; 9–9.10 min, linear gradient back to 100% B; 6 min equilibration wash with 100% B. The flow rate was $0.4\,mL \cdot min^{-1}$. The injection volume was 5 µL. The

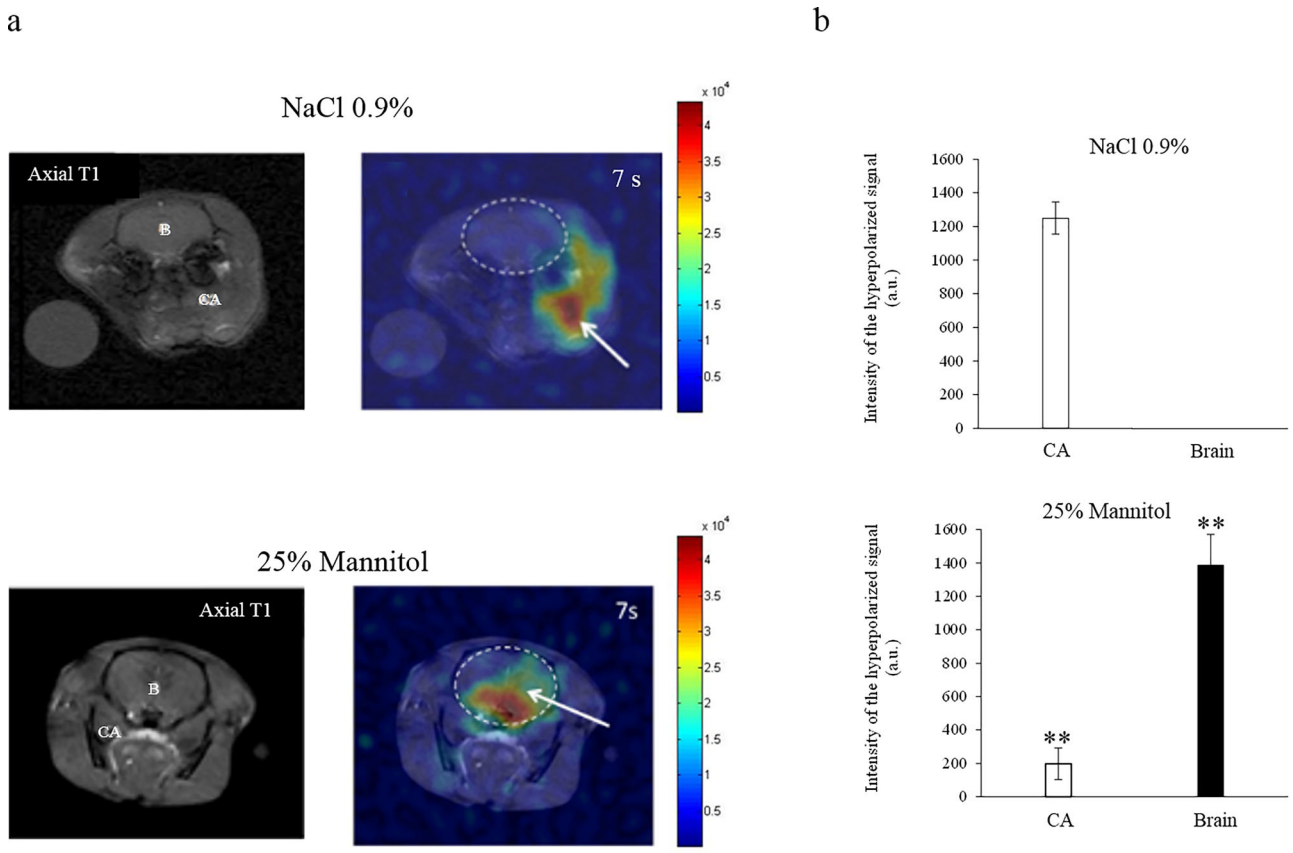

FIG. 1. In vivo detection of hyperpolarized [1-^{13}C]Glu inside the rat brain. Axial T_1-weighted images of rat brain overlaid with representative chemical shift selective images of hyperpolarized [1-^{13}C]Glu. Hyperpolarized [1-^{13}C]Glu signal acquisition was performed using the SPSP sequence centered on the [1-^{13}C]Glu frequency. The main sequence parameters were TR = 3 s and flip angle = 15°. The spatial distribution of Glu is displayed as voxel intensities relative to the maxima. The color scales represent arbitrary linearly distributed intensities for the hyperpolarized images. (**a**)After injection of 0.9% NaCl followed by injection of hyperpolarized [1-^{13}C]Glu in the right CA, the hyperpolarized signal of [1-^{13}C]Glu (white arrows) could be seen only inside the rat head around blood vessels (top). The hyperpolarized signal of [1-^{13}C]Glu (white arrow) was observed in the brain (white dotted circle) only after 25% mannitol infusion (bottom). B, brain; CA, carotid artery; SV, sagittal vein. (**b**) The intensity of the hyperpolarized [1-^{13}C]Glu signal was measured on the color maps at 7 s after the beginning of hyperpolarized [1-^{13}C]Glu injection in a region of interest corresponding to the brain and around the CA. It was normalized to the number of voxels measured. It was expressed in arbitrary units and corresponded to the mean intensity for three rats receiving 25% mannitol before the hyperpolarized [1-^{13}C]Glu injection and for two controls receiving 0.9% NaCl. The hyperpolarized signal was detected in the brain only after 25% mannitol infusion and was confined around the CA after 0.9% NaCl. $^{**}P < 0.01$ versus 0.9% NaCl. Error bars: ± SEM (n = 3 for 25% mannitol group and n = 2 for controls).

column and the autosampler were maintained at 30 °C and 4 °C, respectively. The optimal electrospray ionization source conditions were as follows: capillary tension 4500 V, end plate offset −500 V, nebulizer 40.6 psi, dry gas 9 L · min^{-1}, dry temperature 200 °C. Nitrogen gas was used as desolvation gas. Before analyses, the mass spectrometer was calibrated using a solution of tuning mix.

Post Mortem Analysis

To make sure the carotid occlusion did not induce any brain infarcts during the time of animal installation and NMR in vivo acquisition (~30 min), 2,3,5-triphenyltetrazolium chloride (TTC) staining was used (22). At the end of the hyperpolarized ^{13}C MR experiment, animals (n = 10) were sacrificed. The brains were quickly isolated, placed in a cold (0 °C–4 °C) trough filled with phosphate-buffered saline (PBS) and sectioned in to serial 2-mm-thick coronal slices. The brain slices were held in PBS (<3 min) at room temperature and then transferred to 0.05% TTC incubation medium for 30 min at 37 °C. TTC solutions stained the normal brain tissue in shades of red, while the infarcted tissue remained unstained. Color was assessed qualitatively by direct viewing.

Statistical Analysis

For Evans Blue concentration measurements, intensity of hyperpolarized [1-^{13}C]Glu measured on 2D CSI color maps, signal intensity of hyperpolarized [1-^{13}C]Gln measured on slice-selective spectra, and amount of ^{13}C isotopes ions measured on mass spectra, the results are expressed as the mean ± standard error of the mean (SEM). For LC-MS data, the coefficient of variation was calculated as the difference between the amount of Glu ^{13}C isotope measured in rat brain extracts after [1-^{13}C]Glu and the one measured in control rat brain extracts divided by the amount of Glu ^{13}C measured after [1-^{13}C]Glu and expressed in percentage. Coefficient of variation was also calculated for the Gln ^{13}C isotope.

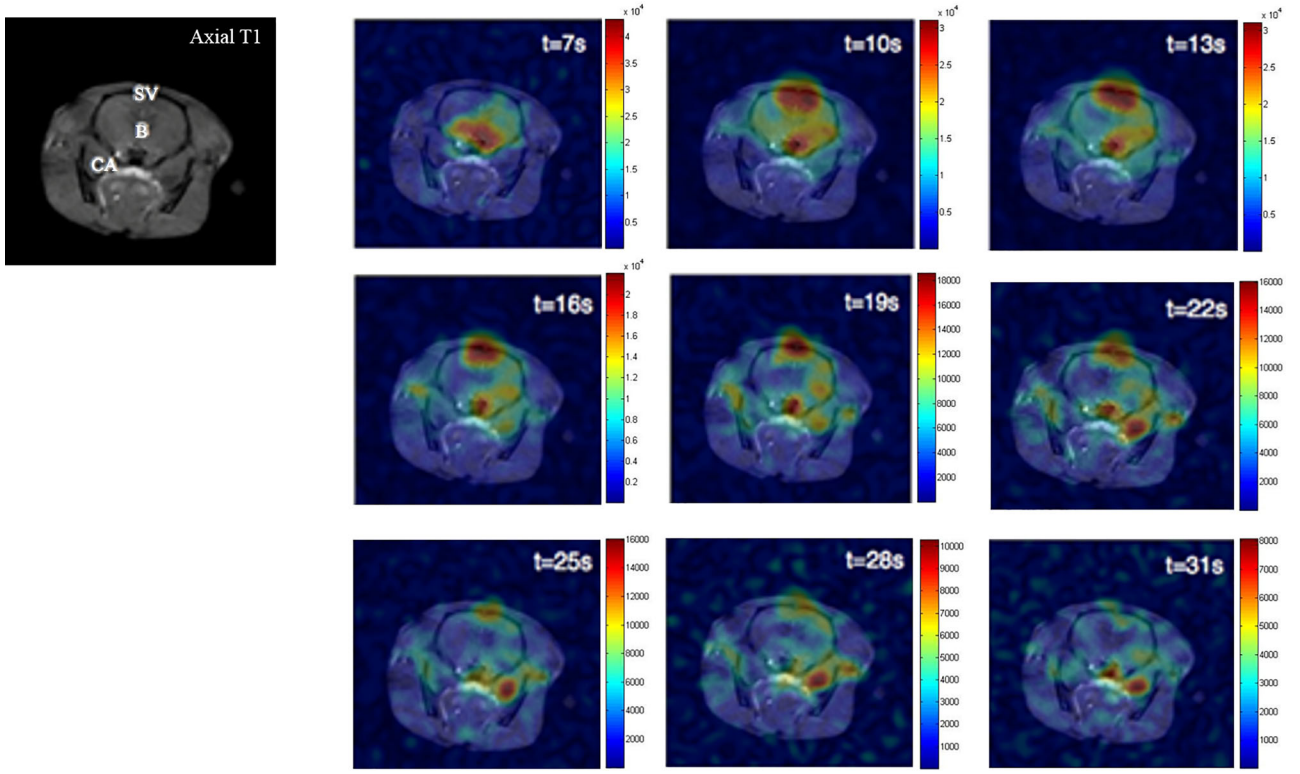

FIG. 2. Time course of the hyperpolarized [1-^{13}C]Glu signal inside the rat brain after 25% mannitol infusion. At 7 s after the beginning of bolus injection, the hyperpolarized signal of [1-^{13}C]Glu appeared first in the carotid artery (CA), then in the brain (B), and finally in an area covering part of the sagittal vein (SV).

Statistical significance was tested using Statistica version 7.1 (Stat Soft, Maisons-Alfort, France) using a Student *t* test.

RESULTS

[1-^{13}C]Glu Dynamic Nuclear Polarization

[1-^{13}C]Glu reached a solid-state polarization of 20% ± 2.3% after a 90-min polarization. After dissolution in the buffered solution, liquid state polarization measured at 37 °C was 13% ± 1.5% (n = 3). The resonances of hyperpolarized [1-^{13}C]Glu (C_1-Glu = 175.4 ppm) and [5-^{13}C]Glu (C_5-Glu = 182.2 ppm) originating from the 1.1% natural abundance of ^{13}C were detected on the in vitro spectra. The relaxation time T_1 of hyperpolarized [1-^{13}C]Glu measured in vitro at 3 T was 30 ± 2.5 s (n = 3).

BBB Opening

The successful opening of the BBB was validated as illustrated by the presence of Evans Blue staining, mainly on the side of injection (Supporting Fig. S3).

In Vivo Visualization of [1-^{13}C]Glu Inside the Brain

SPSP spiral CSI images were acquired every 3 s from the beginning of the hyperpolarized substrate injection. After injection of a 38-mM solution of hyperpolarized [1-^{13}C]Glu, ^{13}C signal was detected inside the right part of the rat brain at 7 s after the beginning of the injection (Fig. 1a). In the animals with a disrupted BBB, hyperpolarized [1-^{13}C]Glu was detected in the brain, unlike in the control group injected with 0.9% NaCl (Fig. 1a). This was confirmed by the measurement of the intensity of the Glu signal performed from the color maps at 7 s after the beginning of the hyperpolarized [1-^{13}C]Glu injection (Fig. 1b).

The Glu images collected from the beginning of the hyperpolarized substrate injection for a rat with a disrupted BBB showed that the Glu signal appeared quickly in the brain 7 s after the beginning of the injection (Fig. 2). Ten seconds after the injection, an elevated Glu signal was also observed in the area covering the sagittal sinus vein. The Glu signal was present inside the brain up to 15 s after the beginning of the acquisition.

The Glu images collected from the beginning of the hyperpolarized substrate injection for a control rat without BBB disruption are presented in Figure 3. Seven seconds after the beginning of the hyperpolarized [1-^{13}C]Glu bolus injection, the Glu signal was mainly localized around blood vessels (Fig. 3). Because the [1-^{13}C]Glu signal was mainly detected around the right CA in each acquisitions, we verified that [1-^{13}C]Glu did not partially diffuse into the healthy brain with time. Twenty-five seconds after the beginning of Glu injection, no more signal was detected maybe due to the dilution of [1-^{13}C]Glu in the systemic circulation.

Synthesis of Hyperpolarized [1-^{13}C]Gln

In this second series of experiments, dynamic ^{13}C spectra were acquired every second from an axial slab containing the whole brain of the rat. Spectra acquisitions were performed after BBB disruption with mannitol to detect hyperpolarized [1-^{13}C]Glu and its metabolites in the brain, and

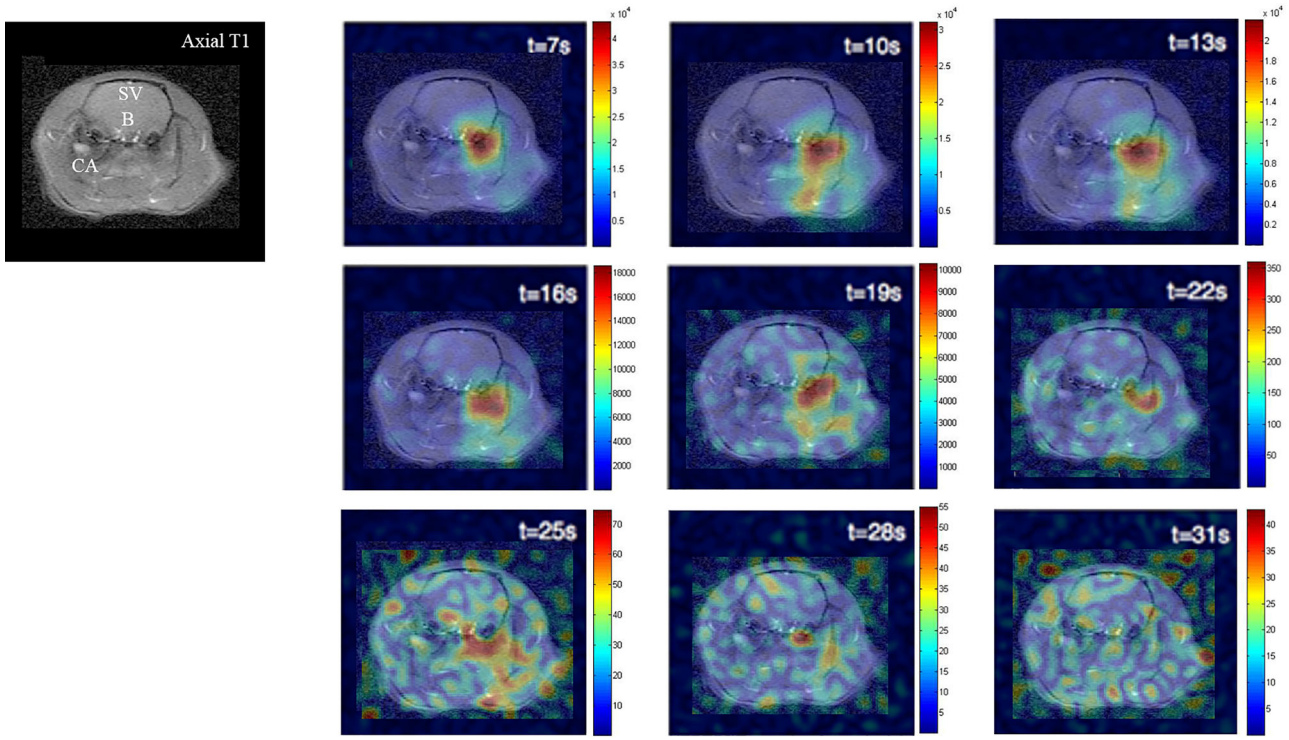

FIG. 3. Time course of the hyperpolarized [1-^{13}C]Glu signal inside the rat brain after NaCl 0.9% infusion. From 7 s after the beginning of hyperpolarized [1-^{13}C]Glu bolus injection to the end of acquisitions, the [1-^{13}C]Glu signal was mainly localized around blood vessels. At 25 s after the beginning of Glu injection, no more signal was detected, likely because of the dilution of [1-^{13}C]Glu in general circulation. B, brain; CA, carotid artery; SV, sagittal vein.

also after NaCl to estimate possible hyperpolarized signals contaminations from surrounding muscles and blood. ^{13}C MRS acquisitions started 7 s after the beginning of the Glu injection to preserve the hyperpolarized signal (Fig. 4a,b).

After mannitol injection, hyperpolarized [1-^{13}C]Glu was injected into the carotid artery; Figure 4e plots the time course of the metabolite signal evolution. The first points were acquired 7 s after the beginning of the bolus injection and were approximately 20 s after the dissolution of hyperpolarized Glu (Fig. 4a,c). The Glu signal was detected as soon as 7 s. The decrease in Glu signal due to T_1 relaxation and metabolic conversion was accompanied by an increase in the [1-^{13}C]Gln signal. The hyperpolarized [1-^{13}C]Glu signal was observed at 175.4 ppm, and a resonance at 174.9 ppm was also detected (Fig. 4a,b). This second resonance may be assigned to [1-^{13}C]Gln due to the delayed appearance of this peak, the well-known metabolism of Glu, and the published chemical shifts of Glu and Gln.

With NaCl injection, the Glu signal was detected at 7 s after injection. The decrease in Glu signal due to T_1 relaxation and metabolic conversion was accompanied by an increase in the [1-^{13}C]Gln signal (Fig. 4b,f). However, in this case, [1-^{13}C]Gln was only detected at the peak, 9 s after Glu bolus injection (Fig. 4f). At this time point, the signal amplitude was half compared to that in rats with disrupted BBB (signal amplitude in arbitrary unit for [1-^{13}C]Gln after NaCl injection and mannitol injection, respectively: 288.6 ± 36.8 versus 558.4 ± 27.2; $P < 0.01$). Furthermore, the decrease in Glu signal was faster after mannitol than after NaCl injection. All of these observations support [1-^{13}C]Glu detection in the brain and a cerebral conversion in [1-^{13}C]Gln. The low [1-^{13}C]Gln signal detection in ras without BBB disruption may be attributed to muscle metabolism and may also reflect free circulating Gln in the blood. The [1-^{13}C]Lac signal present in the phantom was used for frequency and flip angle calibration, and was stable over time.

[1-^{13}C]Glu and [1-^{13}C]Gln detection in the brain were confirmed by the LC-MS chromatogram on rat brain extracts (Fig. 5a). The retention time of Glu is approximately 5.95 min and that of Gln is approximately 6.30 min. In each mass spectrum (Fig. 5b), prominent peaks corresponded respectively to monomer ions with proton $[M+H]^+$ at mass number to charge number ratio (m/z) = 148 for Glu and m/z = 147 for Gln. Lower peaks ($[M+1]^+$ on Fig. 5b) observed at m/z = 149 and m/z = 148 corresponded to the ^{13}C isotopes of Glu and Gln, respectively, with a smaller contribution from isotopes H, O, and N. Ion normalization from the lowest part to the highest part showed that the amount of Glu ^{13}C isotope was significantly higher in rat brain extracts after [1-^{13}C]Glu intracarotid injection than in control rat brain extracts ($8.63\% \pm 0.65\%$ versus $6.11\% \pm 0.21\%$; $P < 0.01$; coefficient of variation $29\% \pm 3\%$) (Fig. 5c). In the same manner, the amount of Gln ^{13}C isotope was significantly higher in rat brain extracts after [1-^{13}C]Glu intracarotid injection than in control rat brain extracts ($8.68\% \pm 0.27\%$ versus $6.18\% \pm 0.13\%$; $P < 0.001$; coefficient of variation $29\% \pm 0.5\%$) (Fig. 5c). Therefore, after BBB disruption, [1-^{13}C]Glu injection induced an increase in Glu and Gln ^{13}C isotopes in the brain. This may reflect astrocytic [1-^{13}C]Glu uptake and its metabolism by Gln synthase to form [1-^{13}C]Gln.

It took an average of 30 min between carotid occlusion and ^{13}C MRS acquisition due to the positioning of

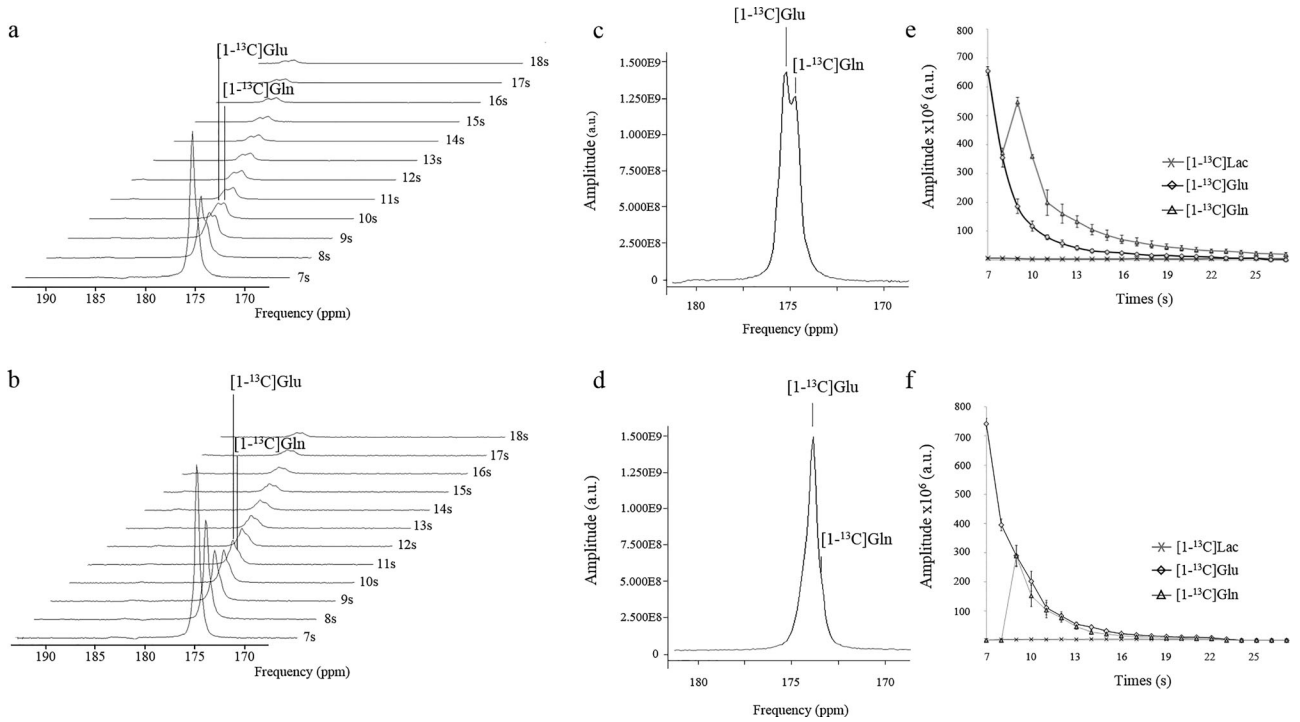

FIG. 4. [1-^{13}C]Glu and [1-^{13}C]Gln can be detected in vivo after BBB opening. (**a, b**) Stack plot representations of the first 12 spectra acquired 7 s after the hyperpolarized [1-^{13}C]Glu injection on a slice covering the rat brain (TR = 1 s; flip angle = 15°). Acquisitions were performed after BBB disruption (a) and after NaCl injection (b). Reference signal from [1-^{13}C]Lac can be seen at 185 ppm. In vivo, the resonance at 175.4 ppm is from [1-^{13}C]Glu, and a [1-^{13}C]Gln peak can be seen at 174.9 ppm. (**c, d**) Sum of the first 10 spectra acquired 7 s after hyperpolarized [1-^{13}C]Glu injection with mannitol (c) and NaCl (d). (**e, f**) In vivo time course of hyperpolarized signals. Signal amplitudes are measured from dynamic ^{13}C spectra acquired on the rat head 7 s after hyperpolarized [1-^{13}C]Glu for three rats that underwent the BBB disruption protocol and three rats without the BBB disruption. At 7 s after injection, hyperpolarized [1-^{13}C]Glu signal was already in an advanced decay state, whereas we observed the appearance of the [1-^{13}C]Gln signal. With mannitol injection, [1-^{13}C]Gln was detected from the 8th second and peaked 9 s after Glu bolus injection (e). After NaCl injection, [1-^{13}C]Gln was only detected at the peak, 9 s after Glu bolus injection (f). At this point, the signal amplitude was half of this measured after BBB disruption. Furthermore, the decrease in Glu signal was faster after mannitol than after NaCl injection. Curves represent averaged amplitudes of hyperpolarized signals of [1-^{13}C]Glu, [1-^{13}C]Gln, and [1-^{13}C]Lac. Error bars: ± SEM.

the animal within the scanner, MR calibrations, and MR image acquisitions. Collected brains at the end of the MRS acquisitions were fully stained with TTC solution, indicating that the ligature of the carotid vessel did not induce brain ischemia in the meantime (Supporting Fig. S4).

DISCUSSION

This study shows that DNP coupled with ^{13}C MRS enabled us to follow the Glu–Gln synthesis to be followed in a time window of few seconds' resolution in the rat brain. By implementing a BBB disruption protocol in healthy rats, this work extends the feasibility of studying brain metabolism with a new range of precursors.

We showed that the injection of hyperpolarized [1-^{13}C]Glu in rats with disrupted BBB lead to its detection inside the rat brain. The SPSP pulse (20) for optimized Glu detection allowed the monitoring of Glu signal inside the rat brain. However, this sequence cannot distinguish Glu and Gln resonances, as the chemical shift difference between C1-labeled Glu and C1-labeled Gln is only 0.5 ppm at 3T. It is possible to increase the spectral resolution by applying our method to higher magnetic field strengths (B0 ≥ 7T). Another way to obtain a better separation of the Glu and Gln peaks is to use [5-^{13}C]Glu as substrate. In fact, labeling the C-5 position produces a larger chemical shift following the conversion to Gln compared with the C-1 position. Unfortunately, we managed to polarize [5-^{13}C]Glu using DNP to modest levels with an average of 13% polarization in the solid state and 5% in the liquid state following dissolution. A second disadvantage was that the T_1 was slightly shorter (27 ± 3 s (n = 3) vs. 30 ± 2.5 s (n = 3) for [5-^{13}C]Glu and [1-^{13}C]Glu, respectively). Consequently, the polarization of [1-^{13}C]Glu, as reported by Gallagher et al. (18), was chosen to validate the current proof-of-concept.

This was done using single-slice ^{13}C NMR experiments that showed that the signal of a metabolite could be detected after hyperpolarized [1-^{13}C]Glu injection at 174.9 ppm. This resonance was assigned to [1-^{13}C]Gln, and this assignment was further confirmed by the chemical shifts of [1-^{13}C]Glu and [1-^{13}C]Gln already published. Because the ^{13}C NMR experiments were conducted on the whole rat head, we cannot exclude a contribution of [1-^{13}C]Glu and [1-^{13}C]Gln from muscles and blood in the recorded signals. Regardless, LC-MS analysis of rat brain extracts confirmed the [1-^{13}C]Gln synthesis from [1-^{13}C]Glu

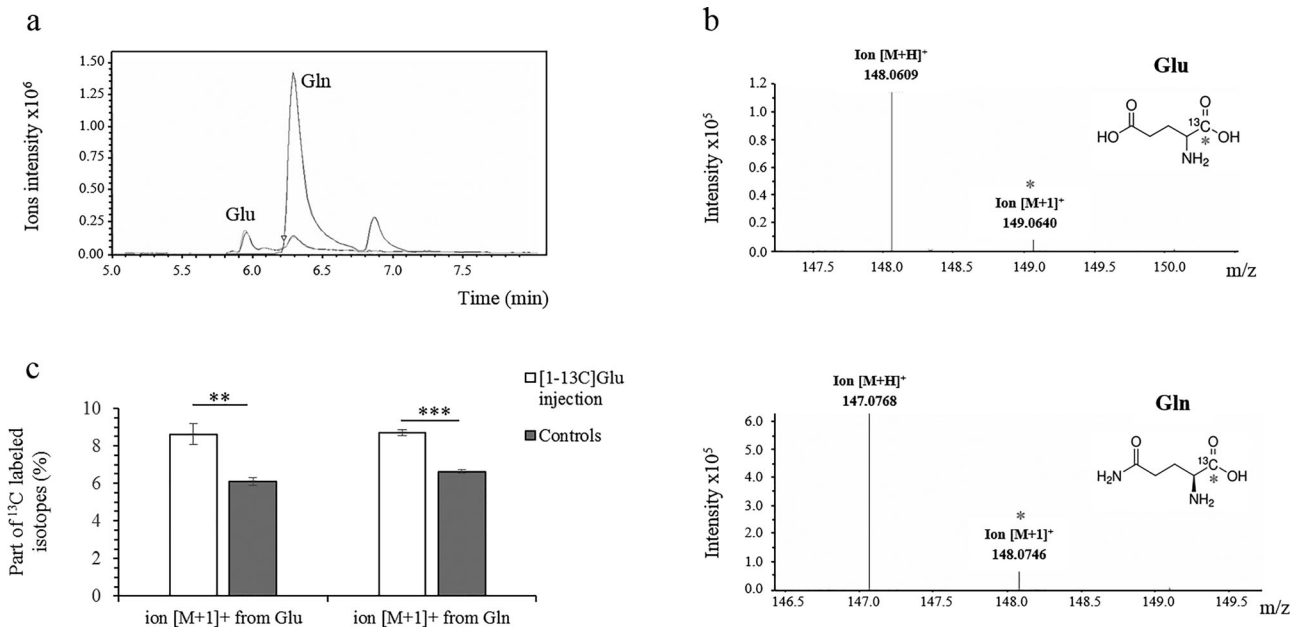

FIG. 5. ^{13}C Glu and ^{13}C Gln detected in rat brain extracts after intracarotid injection of mannitol and [1-^{13}C]Glu. (**a**) Typical extracted-ion chromatogram of Glu and Gln in rat brain extracts. The retention time of Glu is approximately 5.95 min and that of Gln is approximately 6.30 min. (**b**) Glu and Gln mass spectra with prominent peaks, corresponding respectively to monomer ions with proton $[M+H]^+$ of Glu at $m/z = 148$ and Gln at $m/z = 147$. Lower peaks ($[M+1]^+$ with red stars) at $m/z = 149$ and $m/z = 148$ which correspond to the ^{13}C isotopes for Glu and Gln respectively. (**c**) The amount of ^{13}C isotope of Glu and Gln was significantly higher in rat brain extracts after [1-^{13}C]Glu intra-arterial injection ($n = 4$) than in control rat brain extracts ($n = 2$) ($^{**}P < 0.01$ for Glu and $^{***}P < 0.001$ for Gln). Error bars: ± SEM.

inside the rat brains. Furthermore, the differences in kinetic of [1-^{13}C]Glu decay and [1-^{13}C]Gln synthesis acquired in rats with and without BBB disruption protocol supported the hypothesis that a part of the hyperpolarized signals detected may be attributed to the [1-^{13}C]Glu detection in the brain and its cerebral conversion to [1-^{13}C]Gln.

Previous studies using DNP and conducted in the liver showed the detection of AKG signal after the injection of hyperpolarized [1-^{13}C]Glu due to the energy fate of Glu in this organ (18). In the brain, Glu is converted primarily to Gln through Gln synthase in the cytosol of astrocytes. It is reported that an increase in exogeneous Glu concentration leads to preferential Glu metabolism into AKG (23) by the TCA cycle in the brain. Our results suggest that despite BBB disruption, only a small amount of Glu (around 29% of the total Glu injected as coefficients of variation measured on LC-MS spectra) enters the cells. This might be explained by the highly effective Glu transport system efflux present in vivo. In addition, the absence of AKG synthesis might be explained by the cell compartmentation of the mitochondrial Glu dehydrogenase. Consequently, the synthesis into Gln by the cytosolic Gln synthase may be privileged.

Conventional ^{13}C NMR measurements of the uptake and subsequent metabolism of ^{13}C-labeled substrates is a powerful method for studying metabolic fluxes. However, the technique has been hampered by a lack of sensitivity, which has limited both the spatial and temporal resolution. Even at a high magnetic field strength of 14.1 T, the temporal resolution of the ^{13}C NMR experiment is still around 4.5 min (7). The introduction of DNP increases sensitivity to detection and allows temporal and spatial resolutions in the seconds and millimeter ranges, respectively. However, the principal limitation of the technique is the short half-life of the polarization (~20–30 s in vivo), which limits studies to relatively fast metabolic reactions. The current sequence used in our study shows the possibility to detect hyperpolarized [1-^{13}C]Glu inside the brain and the detection of subsequent hyperpolarized [1-^{13}C]Gln in a short period of time.

We achieved a polarization level and a T_1 relaxation of [1-^{13}C]Glu compatible with its detection in vivo (18). Glu has a low solubility in water, hence the sample had to be prepared carefully to maximize sample homogeneity before freezing inside the polarizer to obtain good polarization levels (11). A dissolution step at high pressure and temperature yields a fully dissolved sample that can be injected in animals.

Targeting the central nervous system with labeled precursors is limited by the ability of these agents to gain access to the brain tissue (24). Various methods to overcome this limitation have been described, such as osmotic BBB opening (24,25) or focal BBB opening using ultrasound (26,27). In this study, the hyperpolarized Glu delivery was achieved with 25% mannitol, an osmotic agent widely used for temporary BBB opening (24,28,29). Hypertonic injection induces the rupture of tight junctions between BBB endothelial cells (24). BBB permeability obtained after mannitol infusion is temporary and reverses within 10 min after mannitol injection (24). This is thus compatible with a hyperpolarization experiment.

In animals, the BBB disruption protocol requires a careful considerations, especially in the injection rate and the anesthetic agent (28,30–32). In particular, Remsen et al. (33) reported that during mannitol injection, animals under isoflurane anesthesia presented a lower BBB permeability than under propofol anesthesia. In the present study, temporary BBB disruption was performed as described previously under propofol anesthesia followed by an intracarotid infusion of 25% mannitol at $0.25\,mL \cdot s^{-1} \cdot kg^{-1}$ with no significant neuronal damage (34,35). From Lin et al. (36), regional cerebral blood flow increased in a dose- and time-dependent manner in mannitol-treated rats. With the mannitol dose used here ($1.875\,g \cdot kg^{-1}$), and because measurements were performed around 5 minutes after its injection, we hypothesized that the regional cerebral blood flow was not affected.

BBB permeability was assessed using Evans Blue extravasation. Evans Blue binds to serum albumin rapidly, which in normal physiologic conditions does not cross an intact BBB. The qualitative and quantitative assessments of BBB integrity by macroscopic evaluation (32) and spectrophotometric measurement at 620 nm (36,37) showed a clear disruption of the BBB under our conditions. A small amount of Evans Blue was observed in the contralateral hemisphere of the ligatured artery. This may be explained by the fact that, following a unilateral carotid occlusion, the nonoccluded vessels of the circle of Willis still provide blood to the whole brain.

Usual injections through the internal carotid artery are impractical when the rat is placed inside the scanner. Indeed, this artery cannot be closed temporarily (38). As described previously, we opted to insert the cannula directly inside the main carotid artery (39) after the ligature of its proximal ending. The same route was used to inject the hyperpolarized [1-^{13}C]Glu to prevent a massive hepatic uptake.

Because the NMR experiment lasted around 30 min, ischemia was thus assessed by TTC labeling (22,40) after brain removal. TTC generates a red compound when metabolized by mitochondria and thereby reflects the cell viability. No cerebral ischemia was detected at the time of the experiment.

In conclusion, we have shown a new way to follow the Glu–Gln synthesis in vivo in a time window of few seconds in the brain. This proof-of-concept study shows the feasibility of using hyperpolarized compounds to probe the rat brain by using a prior infusion of hyperosmolar agent.

REFERENCES

1. Ramadan S, Lin A, Stanwell P. Glutamate and glutamine: a review of in vivo MRS in the human brain. NMR Biomed 2013;26:1630–1646.
2. Chassain C, Bielicki G, Donnat JP, Renou JP, Eschalier A, Durif F. Cerebral glutamate metabolism in Parkinson's disease: an in vivo dynamic ^{13}C NMS study in the rat. Exp Neurol 2005;191:276–284.
3. Chassain C, Bielicki G, Keller C, Renou JP, Durif F. Metabolic changes detected in vivo by 1H MRS in the MPTP-intoxicated mouse. NMR Biomed 2010;23:547–553.
4. Rupsingh R, Borrie M, Smith M, Wells JL, Bartha R. Reduced hippocampal glutamate in Alzheimer disease. Neurobiol Aging 2011;32:802–810.
5. Sibson NR, Dhankhar A, Mason GF, Behar KL, Rothman DL, Shulman RG. In vivo 13C NMR measurements of cerebral glutamine synthesis as evidence for glutamate-glutamine cycling. Proc Natl Acad Sci U S A 1997;94:2699–2704.
6. Duarte JM, Gruetter R. Glutamatergic and GABAergic energy metabolism measured in the rat brain by (13) C NMR spectroscopy at 14.1 T. J Neurochem 2013;126:579–590.
7. Lanz B, Xin L, Millet PGR. In vivo quantification of neuro-glial metabolism and glial glutamate concentration using 1H-[13C] MRS at 14.1T. J Neurochem 2014;128:125–139.
8. Ardenkjaer-Larsen JH, Fridlund B, Gram A, Hansson G, Hansson L, Lerche MH et al. Increase in signal-to-noise ratio of > 10,000 times in liquid-state NMR. Proc Natl Acad Sci U S A 2003;100:10158–10163.
9. Golman K, Ardenkjaer-Larsen JH, Petersson JS, Mansson S, Leunbach I. Molecular imaging with endogenous substances. Proc Natl Acad Sci U S A 2003;100:10435–10439.
10. Golman K, in 't Zandt R, Thaning M. Real-time metabolic imaging. Proc Natl Acad Sci U S A 2006;103:11270–11275.
11. Karlsson M, Jensen P, Duus JO, Meier S, Lerche MH. Development of dissolution DNP-MR substrates for metabolic research. Appl Magn Reson 2012;43:223–236.
12. Mishkovsky M, Comment A, Gruetter R. In vivo detection of brain Krebs cycle intermediate by hyperpolarized magnetic resonance. J Cereb Blood Flow Metab 2012;32:2108–2113.
13. Park JM, Josan S, Grafendorfer T, Yen YF, Hurd RE, Spielman DM, Mayer D. Measuring mitochondrial metabolism in rat brain in vivo using MR spectroscopy of hyperpolarized [2-13C] pyruvate. NMR Biomed 2013;26:1197–1203.
14. Marjańska M, Iltis I, Shestov AA, Deelchand DK, Nelson C, Uğurbil K et al. In vivo (13)C spectroscopy in the rat brain using hyperpolarized [1-(13)C]pyruvate and [2-(13)C]pyruvate. J Magn Reson 2010;206:210–218.
15. Butt SA, Søgaard LV, Magnusson PO, et al. Imaging cerebral 2-ketoisocaproate metabolism with hyperpolarized (13)C magnetic resonance spectroscopic imaging. J Cereb Blood Flow Metab 2012;32:1508–1514.
16. Chaumeil MM, Larson PE, Yoshihara HA, et al. Non-invasive in vivo assessment of IDH1 mutational status in glioma. Nat Com 2013;4:1–12.
17. Chaumeil MM, Larson PEZ, Woods SM. Hyperpolarized [1-13C] glutamate: a metabolic imaging biomarker of IDH1 mutational status in glioma. Cancer Res 2014;74:4247–4257.
18. Gallagher FA, Kettunen MI, Day SE, et al. Detection of tumor glutamate metabolism in vivo using (13)C magnetic resonance spectroscopy and hyperpolarized [1-(13)C]glutamate. Magn Reson Med 2011;66:18–23.
19. Schulte RF, Sacolick L, Deppe MH, Janich MA, Schwaiger M, Wild JM, Wiesinger F. Transmit gain calibration for nonproton MR using the Bloch-Siegert shift. NMR Biomed 2011;24:1068–1072.
20. Schulte RF, Sperl JI, Weidl E, et al. Saturation-recovery metabolic-exchange rate imaging with hyperpolarized [1-13 C] pyruvate using spectral-spatial excitation. Magn Reson Med 2013;69:1209–1216.
21. Wiesinger F, Weidl E, Menzel MI, et al. IDEAL spiral CSI for dynamic metabolic MR imaging of hyperpolarized [1-13C] pyruvate. Magn Reson Med 2012;68:8–16.
22. Bederson J, Pitts LH, Tsuji M, Nishimura MC, Davis RL, Bartkowski H. Evaluation of 2,3,5-triphenyltetrazolium chloride as a stain for detection and quantification of experimental cerebral infarction in rats. Stroke 1986;17:1304–1308.
23. Mckenna MC. The glutamate-glutamine cycle is not stoichiometric: fates of glutamate in brain. J Neurosci Res 2007;85:3347–3358.
24. Rapoport SI. Osmotic opening of the blood-brain barrier: principles, mechanism, and therapeutic applications. Cell Mol Neurobiol 2000; 20:217–230.
25. Bellavance MA, Blanchette MFD. Recent advances in blood-brain barrier disruption as a CNS delivery strategy. AAPS J 2008;10:166–177.
26. Kinoshita M, Mcdannold N, Jolesz FA, Hynynen K. Noninvasive localized delivery of Herceptin to the mouse brain by MRI-guided focused ultrasound-induced blood–brain barrier disruption. Proc Natl Acad Sci U S A 2006;103:11719–11723.
27. Aryal M, Arvanitis CD, Alexander PM, McDannold N. Ultrasound-mediated blood–brain barrier disruption for targeted drug delivery in the central nervous system. Adv Drug Delivery Rev 2014;72:94–109.
28. Shawkat H. Mannitol: a review of its clinical uses. BJA Educ 2012;4-7.
29. Blanchette M, Tremblay L, Lepage M, Fortin D. Impact of drug size on brain tumor and brain parenchyma delivery after a blood–brain barrier disruption. J Cereb Blood Flow Metab 2014;34:820–826.
30. Chi OZ, Chun TW, Liu X, Weiss HR. The effects of pentobarbital on blood-brain barrier disruption caused by intracarotid injection of hyperosmolar mannitol in rats. Anesth Analg 1998;86:1230–1235.
31. Chi OZ, Lee DIK, Liu X, Weiss HR. The effects of morphine on blood-brain barrier disruption caused by intracarotid injection of hyperosmolar mannitol in rats. Anesth Analg 2000;90:603–608.

32. Blanchette M, Fortin D. Blood-brain barrier disruption in the treatment of brain tumors. Meth Mol Biol 2011;686:447–463.
33. Remsen LG, Pagel MA, McCormick CI, Fiamengo SA, Sexton GNE. The influence of anesthetic choice, PaCO2, and other factors on osmotic blood-brain barrier disruption in rats with brain tumor xenografts. Anesth Analg 1999;88:559–567.
34. Cosolo WC, Martinello P, Louis WJ, Christophidis N. Blood-brain barrier disruption using mannitol: time course and electron microscopy studies. Am J Physiol 1989;256:443–447.
35. Nicaise C, Mitrecic D, Demetter P, De Decker R, Authelet M, Boom A, Pochet R. Impaired blood-brain and blood-spinal cord barriers in mutant SOD1-linked ALS rat. Brain Res 2009;1301:152–162.
36. Lin W, Paczynski RP, Kuppusamy K, Hsu CY, Haacke EM. Quantitative measurements of regional cerebral blood volume using MRI in rats: effects of arterial carbon dioxide tension and mannitol. Magn Reson Med 1997;38:420–428.
37. Chen KB, Wei VC, Yen LF, et al. Intravenous mannitol does not increase blood-brain barrier permeability to inert dyes in the adult rat forebrain. Neuroreport 2013;24:303–307.
38. Hsieh CH, Chen YF, Chen FD, et al. Evaluation of pharmacokinetics of 4-borono-2- 18 F-fluoro-L-phenylalanine for boron neutron capture therapy in a glioma-bearing rat model with hyperosmolar blood–brain barrier disruption. J Nucl Med 2005;46:1858–1865.
39. Muldoon LL, Pagel MA, Kroll RA, Roman-Goldstein S, Jones RS, Neuwelt EA. A physiological barrier distal to the anatomic blood-brain barrier in a model of transvascular delivery. AJNR Am J Neuroradiol 1999;20:217–222.
40. Chen J, Zhang F. Animal models of acute neurological injuries II. 2012;93–96.

SUPPORTING INFORMATION

Additional Supporting Information may be found in the online version of this article.

Fig. S1. Study design showing timelines for (**a, b**) in vivo ^{13}C NMR acquisitions and (**c, d**) ex vivo validations. (a) Five rats were used for BBB disruption validation by ^{13}C spiral CSI using SPSP scheme (n = 2 with an intracarotidal NaCl + hyperpolarized [1-^{13}C]Glu injections and n = 3 with intracarotidal mannitol + hyperpolarized [1-^{13}C]Glu injections). (b) Six rats were used for the dynamic study of Glu metabolism in the brain using slice-selective ^{13}C NMR spectroscopy on a slice covering the rat head (n = 3 with an intracarotidal NaCl + hyperpolarized [1-^{13}C]Glu injections and n = 3 with intracarotidal mannitol + hyperpolarized [1-^{13}C]Glu injections). (c) Eight rats were used to validate the BBB disruption ex vivo (n = 4 with an intracarotidal 0.9% NaCl injection and n = 4 with intracarotidal injection of a hypertonic solution of 25% mannitol). (d) Six rats were used to validate [1-^{13}C]Glu detection in brain using LC-MS analysis of brain extracts. Four rats received intracarotidal mannitol + [1-^{13}C]Glu injections and two controls received intracarotidal mannitol + 0.9% NaCl.

Fig. S2. Typical spectra obtained after fitting in jMRUI using AMARES algorithm. From bottom to top: experimental spectrum, fitted spectrum, individual metabolite spectra used to generate the fitted spectrum and residual signal of the fitted spectrum.

Fig. S3. BBB opening. Whole brain of samples extracted from one representative animal of each group exposed to mannitol 25% or NaCl 0.9% infusion as assessed by Evans Blue staining (left and right upper figs., respectively) and Evans blue extravasation measured by spectrophotometry at 620 nm (bottom fig.). A blue coloration was visible after mannitol 25% infusion, mainly on the injection side (left upper fig.). BBB disruption was evaluated by spectrophotometry at 620 nm on brain extract to estimate the average Evans Blue extravasation per unit mass ($mg \cdot g^{-1}$ tissue). The results (bottom fig.) showed an increase in Evans Blue concentration inside the hemisphere ipsilateral to injection in rats treated with 25% mannitol compared with controls injected with 0.9% NaCl ($11.12 \pm 2.33\ mg \cdot g^{-1}$ versus $3.96 \pm 0.38\ mg \cdot g^{-1}$; $^{**}P < 0.01$). The Evans Blue concentration is significantly higher in the side of mannitol injection than in the contralateral side ($^{*}P < 0.05$). Error bars: ± SEM (n = 4 for each group).

Fig. S4. Absence of ischemia infract after carotid inclusion illustrated by TTC staining. Representative photograph of TTC stained coronal brain slice of a rat injected with mannitol and hyperpolarized [1-^{13}C]Glu, 55 min after carotid ligation. The fully red-stained brain across the slice shows the absence of ischemia infarct. Scale bar = 1 mm.